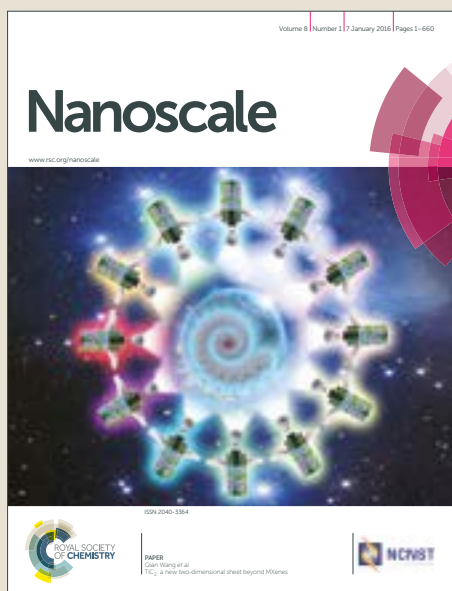


Nanoscale

Accepted Manuscript



This article can be cited before page numbers have been issued, to do this please use: T. Zhang, F. Wang, P. Zhang, Y. Wang, H. Chen, J. Li, J. Wu, C. Li, Z. Chen and S. Li, *Nanoscale*, 2019, DOI: 10.1039/C8NR09900F.



This is an Accepted Manuscript, which has been through the Royal Society of Chemistry peer review process and has been accepted for publication.

Accepted Manuscripts are published online shortly after acceptance, before technical editing, formatting and proof reading. Using this free service, authors can make their results available to the community, in citable form, before we publish the edited article. We will replace this Accepted Manuscript with the edited and formatted Advance Article as soon as it is available.

You can find more information about Accepted Manuscripts in the [author guidelines](#).

Please note that technical editing may introduce minor changes to the text and/or graphics, which may alter content. The journal's standard [Terms & Conditions](#) and the ethical guidelines, outlined in our [author and reviewer resource centre](#), still apply. In no event shall the Royal Society of Chemistry be held responsible for any errors or omissions in this Accepted Manuscript or any consequences arising from the use of any information it contains.

Low-temperature Processed Inorganic Perovskites for Flexible Detectors with Broadband Photoresponse

Ting Zhang^a, Feng Wang^a, Peng Zhang^a, Yafei Wang^a, Hao Chen^a, Jian Li^a, Jiang Wu^{b,c}, Li Chen^{a*}, Zhi David Chen^{a,d}, Shibin Li^{a*}

Received 00th January 20xx,
Accepted 00th January 20xx

DOI: 10.1039/x0xx00000x

www.rsc.org/

Flexible photodetectors (PDs) have become a research hotspot due to their potential applications in foldable displays, wearable optoelectronic devices, and implantable biomedical sensors. Inorganic CsPbBr₃ perovskite, an emerging class of stable metal halide perovskites, are explored as photoactive material in PDs due to its superior photoelectrical property and simple processing. The reported temperature for the fabrication of high quality CsPbBr₃ films is usually higher than 150 °C, which hinders its application to flexible devices. Here, for the first time, high performance flexible PDs based on CsPbBr₃ perovskite films, which show a broadband spectrum response from blind ultraviolet to visible light, are realized via a modified low-temperature (70 °C) solution-processed method. Perovskite films prepared by this method exhibit improved morphology and high light-harvesting capability. The device also yields high on/off ratio (10³), fast response speed (260 ms, rise time) and high responsivity (0.24 mA/W) for solar-blind UV light (254 nm) at 2 V. Moreover, the photodetector exhibits outstanding mechanical flexibility and long-term environmental stability for two months without encapsulation. Our work paves the way for the realization of cost-efficient high-performance flexible optoelectronic devices.

Introduction

Recently, perovskite with crystal structure of ABX₃, where A denotes monovalent cations (e. g. CH₃NH₃⁺ (MA), HC(NH₂)₂⁺ (FA), Cs⁺ or Rb⁺), B denotes bivalent metal cations (Pb²⁺, Sn²⁺ or Ge²⁺), and X denotes halide anions, has been studied as one of the hottest topics in the field of scientific research, material engineering, and photovoltaic devices. The outstanding property of ABX₃, especially hybrid halide perovskites (HHPs), drives an extensive investigation within just few years. Taking perovskite solar cells as an example, since the first reported efficiency of 3.8% in 2009, it has exceeded 23% in less than ten years.^{1,2} Besides, HHPs have shown great potentials in photodetectors (PDs), light emitting diodes (LEDs), and lasers.³⁻¹² For PDs, HHPs are ideal active layer material for possessing desirable physical properties of strong light absorption, long carrier diffusion length, high carrier mobility and low charge recombination rate. However, in spite of these advantageous characteristics, HHPs still face a great bottleneck of stability problem.¹³⁻¹⁷ Since the HHPs are sensitive to heat and humidity,

it is attractive to enhance the stability by replacing the organic component with inorganic cation cesium, leading to a promising class of inorganic cesium lead halide perovskites (IHPs). These materials have garnered much interest within recent two years due to its outstanding photoluminescence and photoelectrical properties.¹⁸⁻²⁰ In particular, cubic α -phase (black perovskite phase) CsPbI₃ with a bandgap of 1.73 eV is an ideal absorber material for inorganic perovskite solar cells (PSCs).^{20,21} Nevertheless, CsPbI₃ is unstable in the black perovskite phase which usually forms at a high temperature above 300 °C and rapidly transforms into a non-perovskite yellow δ -phase in air atmosphere.²¹⁻²⁴ The δ -phase CsPbI₃ possesses a large bandgap of 2.82 eV and results in the degradation of light harvesting. Attempts to stabilize the α -phase via partially substituting I⁻ with Br⁻ have been carried out because the smaller radius of Br anion would reduce the lattice spacing and make the corresponding PSCs more stable.²⁵⁻²⁷ However, the large bandgap (~ 2.0 eV) induced by the presence of Br component is unsuitable for the ideal absorption of solar spectrum. In addition, these CsPbI_{3-x}Br_x perovskites still require a high temperature annealing process (330~350 °C).²⁷

Despite the unsuitable bandgap (2.2 ~ 2.5 eV) for solar cell application with single junction, CsPbBr₃ developed rapidly in the area of PDs and LEDs in the past two years due to their compelling physical properties that include narrow linewidth emission, high quantum yield and high luminescence.^{9,18,28} Moreover, CsPbBr₃ can exist stably at room temperature without any additive treatment. The reported CsPbBr₃ PDs exhibit good environmental stability as well.²⁹⁻³³

It is noted that the majority of high-performance CsPbBr₃ PDs are based on single crystals, microcrystals and two-dimensional

^a School of Optoelectronic Science and Engineering, University of Electronic Science and Technology of China, Chengdu, 610054, China.

^b Department of Electronic and Electrical Engineering, University College London, Torrington Place, London WC1E 7JE, UK

^c Institute of Fundamental and Frontier Sciences, University of Electronic Science and Technology of China, Chengdu, 610054, China.

^d Department of Electrical & Computer Engineering and Center for Nanoscale Science & Engineering, University of Kentucky, Lexington, Kentucky 40506, USA.

Corresponding author: shibinli@uestc.edu.cn; chen_li@uestc.edu.cn.

Electronic Supplementary Information (ESI) available: The supporting information is about experimental details and supporting figures.

Noted: T. Zhang and F. Wang contributed equally to this work.

bulk materials,^{19,23,29,34,35} while thin film based CsPbBr₃ PDs are not well developed. This is because it is yet a challenge to prepare CsPbBr₃ thin films. For one step method, although it is carried out to prepare CsPbBr₃ thin films at low temperature, the obtained film is full of pinholes and not uniform.^{9,22,36} The bad morphology results in an increase of trap-state density and deterioration of carrier transport. Although two step method can produce films with more continuous and homogeneous morphology, the high temperature (usually higher than 150 °C) required for annealing procedure hinders its wider application, especially in flexible devices.^{19,37,38} For instance, polyethylene terephthalate (PET), a widely used flexible substrate, cannot endure high temperature over 100 °C. As a result, it is highly desired to develop a low temperature fabrication method for high quality CsPbBr₃ thin films. Recently, post treatment such as solvent engineering (SE) treatment or solvent-controlled growth techniques was demonstrated to improve the perovskite film quality and the performance of associated solar cells.^{22,23,39} For instance, Luo and co-workers demonstrated a sequential SE treatment to greatly slow down the phase degradation of cubic CsPbI₃ thin films and achieved highly stable CsPbI₃ PSCs.²²

Motivated by the SE treatment applied in CsPbI₃ films, we hypothesize that the quality of CsPbBr₃ would be improved by this method as well. In this work, we demonstrate a modified low-temperature one step method to prepare CsPbBr₃ films for flexible perovskite PDs with broadband photoresponse. The flexible perovskite PDs exhibit a high on/off ratio, fast response speed, excellent mechanical flexibility and improved environmental stability. The results provide a simple and low-cost method to construct the light sensor for a broadband spectrum response from blind ultraviolet to visible light. Moreover, the exploration of flexible CsPbBr₃ PDs may pave a way to extend the application of stable inorganic perovskites to areas including large-area foldable displays, wearable optoelectronic devices, and implantable biomedical devices.

Experimental methods

Materials: Cesium bromide (CsBr, 99.9%), lead bromide (PbBr₂, 99.99%), Dimethyl sulfoxide (DMSO, ≥ 99.9%), chlorobenzene (CBZ, 99.9%), and isopropanol (IPA, ≥ 99.9%) were purchased from Sigma-Aldrich Co. and used directly without purification.

Device Fabrication: Flexible polyethylene terephthalate (PET) substrates were cleaned ultrasonically in acetone, ethanol, deionized water in sequence with each step for 15 min, and dried with nitrogen blowing. 80 nm thick interdigitated Au electrodes were thermally evaporated on PET substrates. The patterned substrates were then exposed to UV-ozone for 15 min before use. A 0.48M CsPbBr₃ precursor solution was prepared by stirring equal molar PbBr₂ and CsBr in anhydrous DMSO at 40 °C for more than 5 h. The CsPbBr₃ precursor solution was spin-coated on the interdigitated electrodes at a speed of 4000 rpm for 30s. To induce fast crystallization, 500 μl CBZ was dropped onto the spinning substrate at the last 5 s of the coating to form perovskite films.² Two different annealing processes were further conducted. For untreated samples, the

obtained perovskite film was annealed at 70 °C for 30 min. For samples with SE treatment, the obtained perovskite film was first annealed at 70 °C for 10 min and then immersed in 70 °C IPA for 5 min and annealed again at 70 °C for 20 min. With the aid of IPA treatment, a relatively high-quality CsPbBr₃ film is obtained. All of the procedures were conducted under ambient conditions at room temperature.

Characterizations and photoresponse measurements: The morphologies of as-prepared films were investigated by field emission scanning electron microscopy (FE-SEM). Atomic force microscopy (AFM) characterizations were conducted on a 300HV scanning force microscope (SEIKO) with tapping mode. The phases and crystallinity of the perovskite films were recorded by X-ray diffraction (XRD) using an X-ray diffractometer (Cu K α radiation, $\lambda=1.54056$ Å). The UV-Vis absorption and steady-state photoluminescence (PL) spectra were performed using a UV-Vis spectrophotometer (Shimadzu UV-3101 PC) and a Hitachi F-4600 fluorescence spectrometer (Edinburgh, FLSP920) with an exciting wavelength of 410 nm, respectively. Time-resolved PL spectra was measured with DCS120 Becker & Hickl confocal scanning FLIM system at an excitation wavelength of 410 nm. The chemical composition analysis was performed by Energy Dispersive X-ray Spectroscopy (EDS), which is equipped on FE-SEM. The current – voltage (I-V) curves were measured by a Keithley 4200 Semiconductor Parametric Analyzer under illumination of different light sources (254, 365, 450, 540 and 550 nm). The incident light intensity was recorded using a commercial power meter (Thorlabs PM 100D). EQE and responsivity were obtained by QE-R measurement system (Enli tech from Taiwan) equipped with a calibrated silicon PD as reference. All the measurements were performed under ambient conditions at room temperature.

Results and discussion

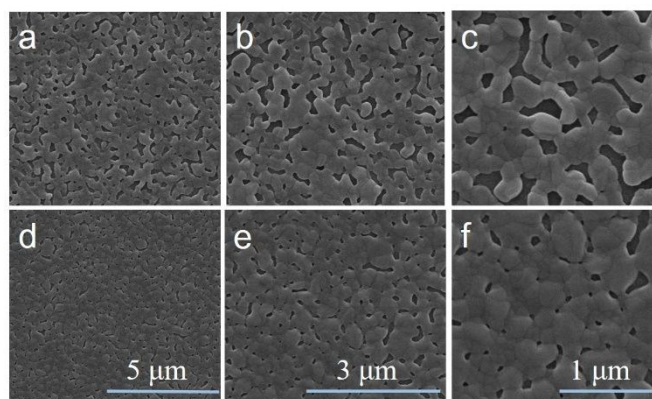


Figure 1. Top-view SEM images of the CsPbBr₃ films (a), (b), (c) without SE treatment (d), (e), (f) with SE treatment under different magnifications.

Herein, we utilized one step method with a low annealing temperature of 70 °C to prepare CsPbBr₃ perovskite films. The preparation of CsBr-DMSO-PbBr₂ precursor solution was conducted by continuously stirring it at 40 °C for more than 5 h. It should be noted that no surfactant was used here.

Surfactants, which are often added into the precursor to achieve a high dissolution, will act as drifting obstacles for carriers. It is important to mix equal molar quantities of CsBr and PbBr₂ in the precursor, because non-stoichiometric CsBr/PbBr₂ precursors will form diverse cesium lead bromide perovskite reactants, including CsPb₂Br₅, CsPbBr₃ and Cs₄PbBr₆.^{9,40} The scanning electron microscopy (SEM) pictures of obtained CsPbBr₃ film with or without SE treatment were compared. As shown in Figure 1a-c, the pristine CsPbBr₃ film was discontinuous and possessed numerous large pinholes. After SE treatment, morphology of the film (Figure 1d-f) was greatly improved showing higher coverage and less and smaller pinholes. It is noted the treated film in Figure 1 was obtained with an optimized SE treatment process. As shown in Figure S1, SEM results reveal the effect of various duration for the first step annealing and immersion on the final morphology. It was found 10 mins for the first step annealing and 5 mins for IPA immersion were the optimal conditions. The optimized SE treatment process was adopted to prepare treated CsPbBr₃ film throughout this work.

Atomic force microscopy (AFM) characterization was also conducted to compare the surface morphology of pristine and SE treated CsPbBr₃ films. As depicted in Figure S2 (Supporting Information), the root-mean square (RMS) roughness of the perovskite films with or without SE treatment were 22.491 nm and 34.228 nm, respectively. The AFM analysis shows that the SE treatment yields a smoother surface.

To further check the crystal structure and phase purity of prepared CsPbBr₃ films, X-ray diffraction (XRD) patterns were recorded as shown in Figure 2a. For the films treated with SE, peaks at 15.06°, 21.5°, 30.62°, 33.74°, and 37.78° can be assigned to the (001), (010), (002), (-112) and (102) crystallographic planes of CsPbBr₃, respectively. The XRD spectra here show an orthorhombic unit cell in space group Pnma (3D perovskite structure), which matches well with the XRD patterns of CsPbBr₃ films as previously reported.^{19,22} In contrast, in the case of untreated CsPbBr₃ film, a peak at 11.7° exists obviously, which may belong to the phase of CsPb₂Br₅ or PbBr₂.^{41,42} The XRD results demonstrate that the SE treatment can enhance the phase purity of CsPbBr₃ films. Moreover, a quantitative analysis for elemental composition of the SE treated CsPbBr₃ film was performed by using energy dispersive X-ray spectroscopy (EDS). As shown in Figure S3 (Supporting Information), we can clearly identify the chemical compositions (Cs, Pb and Br) from the EDS spectra. The integration of the elemental characteristic peaks demonstrates a quantified atomic ratio (%) of 21.02(1):18.49(1): 60.49(3) for Cs:Pb:Br, which is in accordance with the ideal stoichiometric ratio of CsPbBr₃. The optical properties of CsPbBr₃ films with or without SE treatment were investigated by Ultraviolet-visible (UV-Vis) absorption and steady-state photoluminescence (PL) techniques. For absorption, both samples presented a strong peak at 516 nm and a sharp edge at 530 nm, as displayed in Figure 2b. The absorption feature of the CsPbBr₃ films indicates it can be used as an active layer for visible photodetection, especially in green light region. It is evident that the absorption of perovskite films with SE treatment was enhanced.

Additionally, an absorption bandgap of ~ 2.28 eV was determined using Tauc plot method (shown in Figure S4, supporting information). The measured absorption edge is in good agreement with the

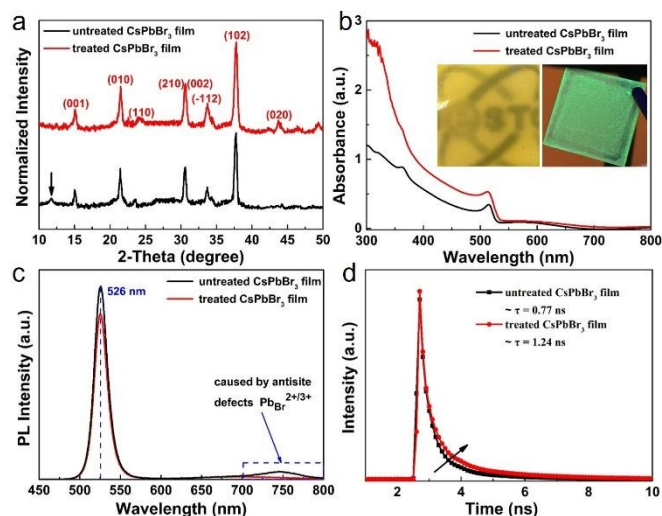


Figure 2. Comparison of (a) XRD patterns, (b) absorption, (c) photoluminescence spectra, and (d) time-resolved photoluminescence decay curves of CsPbBr₃ films with or without SE treatment. Insets in Figure 2 (b) show photograph of the CsPbBr₃ layer under ambient light (left) and UV lamp (right), respectively.

dominant PL emission peak at 526 nm for both untreated and treated perovskite film, as shown in Figure 2c. From the steady-state PL spectra, clearly there was a broad emission peak located at ~ 747 nm for the untreated CsPbBr₃ film. According to first-principles calculation, this emission feature is induced by antisite Pb_{Br}^{2+/3+}, a kind of intrinsic point defect in CsPbBr₃.⁴³ Such a defect can introduce deep transition levels to emit luminescence even at near-infrared wavelengths. Upon solvent treatment, this ~ 747 nm emission peak was quenched substantially, suggesting that those defects were effectively passivated. In addition, the dominant emission peak was reduced slightly, indicating a lower PL quantum yield. We further studied charge carrier dynamics through measuring the time-resolved PL. As depicted in Figure 2d, the treated perovskite film exhibited slower decay behavior. The average lifetimes (τ) for pristine and treated CsPbBr₃ film were extracted to be 0.77 and 1.24 ns, respectively. The extended fluorescence lifetime of the treated CsPbBr₃ film indicates reduced nonradiative defect density. Once the photoactive layer absorbs illumination light, the photogenerated electron-hole pairs will accumulate and recombine within the lifetime in CsPbBr₃ film. During the above-mentioned transient process of charge carriers, the photons will be produced and released to form the PL spectrum, which corresponds to an optical bandgap of the CsPbBr₃ film. The improved absorption and PL results indicate that the modified low temperature one-step method reduced the defect-induced deep transition levels. This method can serve as a guidance for experimental synthesis of relatively high-quality CsPbBr₃ films.

After confirmed the enhanced properties of the treated CsPbBr₃ film, we further measured the photo-electric properties of the CsPbBr₃ based flexible PDs with SE treatment. Figure 3a shows the diagram of the fabrication process of flexible PDs. The porous CsPbBr₃ films were prepared on a pre-patterned polyethylene terephthalate (PET) substrate with interdigitated gold electrodes. The energy level alignment between CsPbBr₃ and gold electrode is illustrated in Figure 3b. As the work function of Au electrode is high, the Au-CsPbBr₃ interfaces would form a good ohmic contact.⁴⁴ Figure 3c shows typical current-voltage (*I*-*V*) curves of the device based on a SE treated CsPbBr₃ film in the dark and under illumination by 450 nm laser diode (LD) source at various illumination intensities. Consistently, the *I*-*V* curves show a linear behavior, further demonstrating that the good ohmic contact was formed between perovskite films and electrodes. The flexible photodetector based on an untreated CsPbBr₃ film showed a weak photocurrent response under 450 nm light illumination at 1 V bias (Figure S5a and b, Supporting Information), and a higher dark current (100 nA at 1 V bias) (Figure S5a, Supporting Information). In comparison, the photodetector based on a SE treated CsPbBr₃ film showed a relatively weaker dark current at 1 V bias (48 nA) and a good photocurrent response when it was exposed to a 450 nm light illumination at a bias of 2 V. The result further confirms that the perovskite layer treated by SE technique exhibited more efficient light harvesting and faster charge transfer, thus enhancing the photocurrent response of the device.

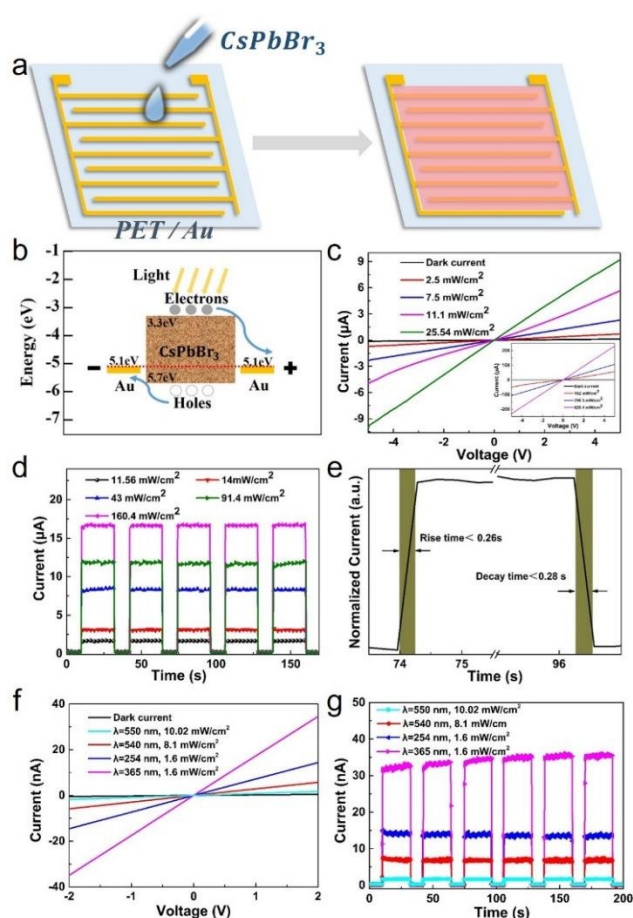


Figure 3. Optoelectronic performance of SE treated CsPbBr₃ flexible PDs. (a) Schematic illustration of the fabrication of flexible PDs with CsPbBr₃ photoactive layer; (b) Schematic diagram of energy levels of the PDs; (c) Current-voltage characteristics of the flexible device under dark and different light intensities with a 450 nm laser diode. Inset stands for the current-voltage characteristics at higher incident light intensities. (d) Temporal photoresponse of the device under 450 nm irradiation at different intensities when biased at 2 V. (e) Normalized transient photoresponse. (f) *I*-*V* (g) and *I*-*t* curves of the device at different light sources (254, 365, 540, 550 nm).

To further check the photoelectrical response characteristics of our flexible PDs, time dependent photocurrents (*I*-*t*) were measured and plotted, as shown in Figure 3d. Upon light irradiation, the photocurrent raised immediately, and then decreased rapidly when the light was sheltered. Under 0.62 W/cm² illumination, the current enhanced three orders of magnitude, leading to a high on/off ratio of $\sim 10^3$, which indicates that the flexible photodetector exhibits a good light-switching behavior. Figure S6 (Supporting Information) shows that the device exhibited a reproducible photocurrent response to periodic on/off light after being exposed to light illumination over 3000 s. It can be seen that the device still showed a very good photocurrent reproducibility and stability to periodic intermittent light illumination. The photocurrent (I_{ph}) as a function of the incident light intensity (P) is shown in Figure S7 (Supporting Information). When the light was applied to irradiate the active area, the current increased sublinearly with the incident light intensity from 2.5 to 620.4 mW/cm² due to the increase of photogenerated carriers. The increase trend can be fitted by an approximate law equation of $I_{ph} \approx aP^\alpha$, where a is proportionality constant, α stands for the index of power law. For our device, the calculated α is 0.89, which is deviated from the ideal index ($\alpha = 1$). The deviation might result from the trap states presented in the film, which would form recombination centers for electrons and holes. This phenomenon has also been reported and investigated in previous perovskite PDs.³⁰

To evaluate the response speed of the flexible photodetector, we investigated transient photocurrent of the device, as shown in Figure 3e. The rise time is defined as the time spent on rising from 10% of maximum photocurrent to 90%, and vice versa for the decay time. In Figure 3e, the rise time and decay time are extracted to be shorter than 0.26 and 0.28 s, respectively. Compared with the previous reports on response speed of CsPbBr₃ film,³⁶ the performance of our device is much better. The fast response behavior can be primarily ascribed to the efficient charge separation and collection, which are affected by the carrier mobility and the interface of semiconductor/metal. The ohmic contact between perovskite films and electrodes effectively decreases the contact barrier, resulting in a fast transport path for charge carriers. The respond speed is therefore enhanced.

Responsivity, which is a critical parameter for a detector, is defined as the photocurrent generated per unit intensity of the incident light. It is expressed as the following formula:

$$R = \frac{I_{ph}}{L_{light}}$$

Where J_{ph} is the photocurrent, L_{light} is the incident light intensity. R reflects how efficiently the detector responds to the light signals. It is observed that the responsivity monotonously decreased with the increasing incident light intensity (shown in Figure S8, Supporting Information). Accordingly, at a low light intensity (2.5 mW/cm^2), a responsivity of 2.9 mA/W for our device was obtained under 450 nm illumination with a bias of 1 V . As a key figure-of-merit parameter for further characterizing the performance of PDs, specific detectivity (D^*) is related to its noise current and responsivity. For a photoconductive photodetector, shot noise is assumed to be the dominant contribution to the total noise.⁴ Therefore, D^* can be calculated by $D^* = \frac{R}{(2qI_d)^{1/2}}$ and plotted in Figure S8, where I_d is the dark current. The corresponding D^* was about 10^{10} Jones (Jones = $\text{cm} \times \text{Hz}^{1/2} \times \text{W}^{-1}$). The high detectivity is attributed to the improved film quality through SE treatment. Further, we compared the photoelectric properties of our device with other perovskite PDs and the corresponding data were briefly summarized in Table S1 (Supporting Information).

We next investigated the light response of our device by measuring the photo-electric characteristics under different light sources (wavelength includes 254 , 365 and 540 nm). As shown in Figure 3f, with UV ($\lambda = 254, 365 \text{ nm}$) illumination intensity increased from dark to 1.6 mW/cm^2 , the photocurrent increased to 15 and 35 nA at 2 V respectively. The corresponding current on/off ratios were 29 and 70 , respectively. The results demonstrate that the CsPbBr_3 film as a photoactive layer is a promising alternative to be used for the application of visible blind UV detectors. Under 540 nm LD irradiation (8.1 mW/cm^2), the detector outputted a weak photocurrent as shown in Figure 3f. The obtained current on/off ratio was about 10 at 2 V . It is well known that the mechanism of photoconductive detector is based on the generation of photoexcited electron-hole pairs once semiconductors absorb the incident light with photon energy higher than its bandgap. Light with larger photon energy in the short wavelength can excite electrons from the valence band to the conduction band and form excitons. Both electrons and holes, namely free carriers are disassociated from the excitons, will be driven outside the perovskite film and injected into the electrodes under the built-in field or applied voltage, thus contributing to an output photocurrent. It is evident that the generated photocurrent exhibited a large decrease at 540 nm , which is close to the optical bandgap of CsPbBr_3 . The responsivity of the device under 254 nm (UV-blind), 365 nm (UV) and 540 nm (Vis) wavelength light irradiation was calculated to be 0.24 , 0.55 , 0.02 mA/W , respectively. High detectivity of 1.9×10^{10} , 4.4×10^{10} , 1.6×10^9 Jones, respectively, was achieved for our device. The obscure photoresponse at 550 nm may result from the defects, which exists in perovskite film and introduces energy levels in forbidden band, thus leading to photons with energy less than its bandgap be absorbed.⁴⁵ To further check the photon response at various wavelengths, external quantum efficiency (EQE) was measured at different biases. As shown in Figure S9a, the EQE increased as the increasing bias. Obviously, the obtained spectra agree well with the absorption curves depicted in Figure 2b. The corresponding responsivity was

calculated and plotted in Figure S9b. I-t curves depicted in Figure 3g fit well with the dark and light current (shown in Figure 3f) curves, indicating the PDs based on inorganic perovskite CsPbBr_3 have a fast response speed and negligible delay property. The excellent photoresponse characteristics demonstrate that the CsPbBr_3 photodetector holds a great potential in the application of solar blind-UV detection.

Mechanical flexibility is an important factor affecting the practical application in wearable electronic devices. As depicted in Figure 4, we measured the dependence of photo-electric performance on curvature radii and bending cycles. All measurements were carried out in air atmosphere without any device encapsulation. The photographic images in the inset of Figure 4a show different bending states of the tested flexible PD under various bending radii of 19.94 , 15.16 , 9.56 , 5.12 mm , respectively. The photocurrent shown in Figure 4a remained almost unchanged at different curvature radii under a biased voltage of 2 V , which demonstrates that our flexible PD was not influenced by the stress of external bending moments. Figure 4b depicts the I-V features after different bending cycles at a bending angle of 30° (definition of bending angle is provided in the inset of Figure 4b). It is clear that the flexible photodetector showed a stable and reproducible photocurrent response ($0.26 \mu\text{A}$) to periodic on/off light after 220 bending cycles (shown in Figure 4c). Compared with its initial photocurrent of $0.29 \mu\text{A}$ before bending, a small performance fluctuation of 10% was exhibited. Furthermore, even at deflected conditions, the photocurrent response also can be measured, as shown in Figure S10. The obvious current decrease is ascribed to the less active area at the bending radii of 1.05 mm condition.

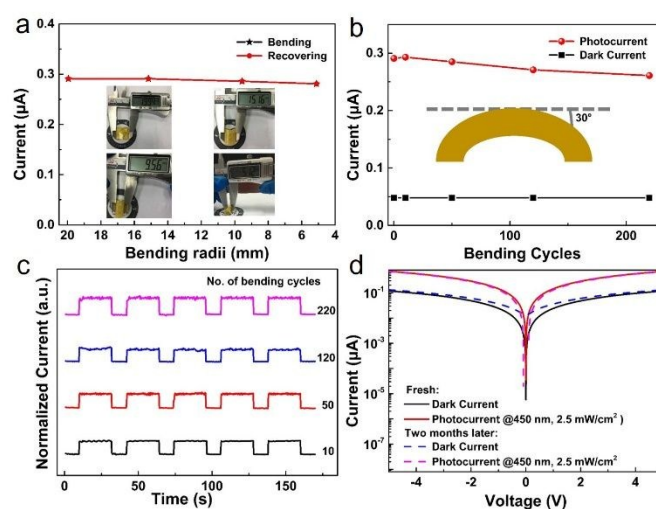


Figure 4. (a) I-V curves of the flexible device at different bending curvatures when biased at 2 V . It shows an excellent optoelectronic performance stability when the flexible device undergoes a bending-recovery cycle. (b) Photocurrent variation after different repeated bending cycles at a specific bending angle of 30° , and the inset is a schematic diagram of the bending angle. (c) I-t curves of the flexible photodetector after different bending cycles under a bias voltage of 2 V . (d) Comparison of dark and photo-current of our device kept for two months in ambient air at $35 \sim 45\%$ relative humidity.

Additionally, the environmental stability of our photodetector was tested by measuring the photocurrent response of a device to 450 nm light (2.5 mW cm^{-2}) after being stored for two months in ambient conditions at 35~45% relative humidity. As shown in Figure 4d and Figure S11a, the dark current, photocurrent and time-dependent photoresponse of the device show a negligible change (~2% decrease), which could be resulted from experimental run-to-run errors. Figure S11b also displays optical photos and absorption curves of the device as-prepared and aged, confirming a good stability in ambient air. The high stability of our device indicates that our solution-processed CsPbBr₃ films may have practical application in optoelectronic PDs and switches.

Conclusions

In summary, the all inorganic halide perovskite flexible PDs based on CsPbBr₃ film are fabricated by a modified low temperature, and solution-processed strategy. The flexible PDs show a broadband spectrum response from blind ultraviolet to visible light with a high on/off ratio, fast response speed, and excellent stability. Such a good photoresponse property is ascribed to the improved morphology prepared by SE technique, which can provide both efficient light-harvesting and high charge transfer ability. The results provide a great promise for the application of CsPbBr₃ perovskite in broadband detection, especially for solar-blind UV light on flexible substrates.

Conflicts of interest

There are no conflicts to declare.

Acknowledgements

This work was supported by National Natural Science Foundation of China under Grant Nos. 61421002, 61874150, 61574029, and 61471085. This work was also partially supported by University of Kentucky.

Notes and references

- 1 A. Kojima, K. Teshima, Y. Shirai, T. Miyasaka, *J. Am. Chem. Soc.* 2009, **131**, 6050–6051.
- 2 N. J. Jeon, H. Na, E. H. Jung, T.-Y. Yang, Y. G. Lee, G. Kim, H.-W. Shin, S. Il Seok, J. Lee, J. Seo, *Nat. Energy* 2018, **3**, 682–689.
- 3 H. Wang, D. H. Kim, *Chem. Soc. Rev.* 2017, **46**, 5204–5236.
- 4 T. Zhang, J. Wu, P. Zhang, W. Ahmad, Y. Wang, M. Alqahtani, H. Chen, C. Gao, Z. D. Chen, Z. Wang, S. Li, *Adv. Opt. Mater.* 2018, **6**, 1–8.
- 5 Y. Wang, Y. Zhang, Y. Lu, W. Xu, H. Mu, C. Chen, H. Qiao, J. Song, S. Li, B. Sun, Y.-B. Cheng, Q. Bao, *Adv. Opt. Mater.* 2015, **3**, 1389–1396.
- 6 S. Chen, G. Shi, *Adv. Mater.* 2017, **29**, 1–31.
- 7 Y. Fang, Q. Dong, Y. Shao, Y. Yuan, J. Huang, *Nat. Photonics* 2015, **9**, 679–686. DOI: 10.1039/C8NR09900F
- 8 X. Xu, C.-C. Chueh, P. Jing, Z. Yang, X. Shi, T. Zhao, L. Y. Lin, A. K.-Y. Jen, *Adv. Funct. Mater.* 2017, **27**, 1–6.
- 9 N. Yantara, S. Bhaumik, F. Yan, D. Sabba, H. A. Dewi, N. Mathews, P. P. Boix, H. V. Demir, S. Mhaisalkar, *J. Phys. Chem. Lett.* 2015, **6**, 4360–4364.
- 10 S. D. Stranks, H. J. Snaith, *Nat. Nanotechnol.* 2015, **10**, 391–402.
- 11 W. Hu, W. Huang, S. Yang, X. Wang, Z. Jiang, X. Zhu, H. Zhou, H. Liu, Q. Zhang, X. Zhuang, J. Yang, D. H. Kim and A. Pan, *Adv. Mater.* 2017, **29**, 1–8.
- 12 Q. Zhang, R. Su, W. Du, X. Liu, L. Zhao, S. T. Ha, Q. Xiong, *Small Methods* 2017, **1**, 1700163.
- 13 M. Shahbazi, H. Wang, *Sol. Energy* 2016, **123**, 74–87.
- 14 X. Tong, F. Lin, J. Wu, Z. M. Wang, *Adv. Sci.* 2015, **3**, 1–18.
- 15 Y. Zhao, K. Zhu, *Chem. Soc. Rev.* 2016, **45**, 655–689
- 16 J. Yang, T. L. Kelly, *Inorg. Chem.* 2017, **56**, 92–101.
- 17 P. Zhang, J. Wu, T. Zhang, Y. Wang, D. Liu, H. Chen, L. Ji, C. Liu, W. Ahmad, Z. D. Chen, S. Li, *Adv. Mater.* 2018, **30**, 1–20.
- 18 X. Li, F. Cao, D. Yu, J. Chen, Z. Sun, Y. Shen, Y. Zhu, L. Wang, Y. Wei, Y. Wu, H. Zeng, *Small* 2017, **13**, 1–24.
- 19 B. Yang, F. Zhang, J. Chen, S. Yang, X. Xia, T. Pullerts, W. Deng, K. Han, *Adv. Mater.* 2017, **29**, 1–8.
- 20 A. Swarnkar, A. R. Marshall, E. M. Sanehira, B. D. Chernomordik, D. T. Moore, J. A. Christians, T. Chakrabarti, J. M. Luther, *Science* 2016, **354**, 92–95.
- 21 G. E. Eperon, G. M. Paterno, R. J. Sutton, A. Zampetti, A. A. Haghighirad, F. Cacialli, H. J. Snaith, *J. Mater. Chem. A* 2015, **3**, 19688–19695.
- 22 P. Luo, W. Xia, S. Zhou, L. Sun, J. Cheng, C. Xu, Y. Lu, *J. Phys. Chem. Lett.* 2016, **7**, 3603–3608.
- 23 P. Wang, X. Zhang, Y. Zhou, Q. Jiang, Q. Ye, Z. Chu, X. Li, X. Yang, Z. Yin, J. You, *Nat. Commun.* 2018, **9**, 1–7.
- 24 L. A. Frolova, D. V. Anokhin, A. A. Piryazev, S. Y. Luchkin, N. N. Dremova, K. J. Stevenson, P. A. Troshin, *J. Phys. Chem. Lett.* 2017, **8**, 67–72.
- 25 L. Yan, Q. Xue, M. Liu, Z. Zhu, J. Tian, Z. Li, Z. Chen, Z. Chen, H. Yan, H.-L. Yip, Y. Cao, *Adv. Mater.* 2018, **30**, 1–7.
- 26 C.-Y. Chen, H.-Y. Lin, K.-M. Chiang, W.-L. Tsai, Y.-C. Huang, C.-S. Tsao, H.-W. Lin, *Adv. Mater.* 2017, **29**, 1–7.
- 27 R. J. Sutton, G. E. Eperon, L. Miranda, E. S. Parrott, B. A. Kamino, J. B. Patel, M. T. Horantner, M. B. Johnston, A. A. Haghighirad, D. T. Moore, H. J. Snaith, *Adv. Energy Mater.* 2016, **6**, 1–6.
- 28 Z. Wei, A. Perumal, R. Su, S. Sushant, J. Xing, Q. Zhang, S. T. Tan, H. V. Demir, Q. Xiong, *Nanoscale* 2016, **8**, 18021–18026.
- 29 J. Song, L. Xu, J. Li, J. Xue, Y. Dong, X. Li, H. Zeng, *Adv. Mater.* 2016, **28**, 4861–4869.
- 30 G. Tong, H. Li, D. Li, Z. Zhu, E. Xu, G. Li, L. Yu, J. Xu, Y. Jiang, *Small* 2018, **14**, 1–8.
- 31 F. Cao, D. Yu, X. Li, Y. Zhu, Z. Sun, Y. Shen, Y. Wu, Y. Wei, H. Zeng, *J. Mater. Chem. C*, 2017, **5**, 7441.
- 32 X. Li, D. Yu, J. Chen, Y. Wang, F. Cao, Y. Wei, Y. Wu, L. Wang, Y. Zhu, Z. Sun, J. Ji, Y. Shen, H. Sun, H. Zeng, *ACS Nano* 2017, **11**, 2015–2023.

- 33 J. Zeng, X. Li, Y. Wu, D. Yang, Z. Sun, Z. Song, H. Wang, H. Zeng, *Adv. Funct. Mater.* 2018, **28**, 1804394.
- 34 M. I. Saidaminov, M. A. Haque, J. Almutlaq, S. Sarmah, X.-H. Miao, R. Begum, A. A. Zhumekenov, I. Dursun, N. Cho, B. Murali, O. F. Mohammed, T. Wu, O. M. Bakr, *Adv. Opt. Mater.* 2017, **5**, 1600704.
- 35 L. Li, Z. Sun, P. Wang, W. Hu, S. Wang, C. Ji, M. Hong, J. Luo, *Angew. Chem.* 2017, **129**, 12318–12322.
- 36 C. Li, C. Han, Y. Zhang, Z. Zang, M. Wang, X. Tang, J. Du, *Sol. Energy Mater. Sol. Cells* 2017, **172**, 341–346.
- 37 J. Liang, C. Wang, Y. Wang, Z. Xu, Z. Lu, Y. Ma, H. Zhu, Y. Hu, C. Xiao, X. Yi, G. Zhu, H. Lv, L. Ma, T. Chen, Z. Tie, Z. Jin, J. Liu, *J. Am. Chem. Soc.* 2016, **138**, 15829–15832.
- 38 M. Kulbak, S. Gupta, N. Kedem, I. Levine, T. Bendikov, G. Hodes, D. Cahen, *J. Phys. Chem. Lett.* 2016, **7**, 167–172.
- 39 Z. Xiao, Q. Dong, C. Bi, Y. Shao, Y. Yuan, J. Huang, *Adv. Mater.* 2014, **26**, 6503–6509.
- 40 J. Xue, Y. Gu, Q. Shan, Y. Zou, J. Song, L. Xu, Y. Dong, J. Li, H. Zeng, *Angew. Chem. Int. Ed.* 2017, **56**, 5232–5236.
- 41 X. Zhang, Z. Jin, J. Zhang, D. Bai, H. Bian, K. Wang, J. Sun, Q. Wang, S. F. Liu, *ACS Appl. Mater. Interfaces* 2018, **10**, 7145.
- 42 Z. Zhang, Y. Zhu, W. Wang, W. Zheng, R. Lin, F. Huang, *J. Mater. Chem. C* 2018, **6**, 446.
- 43 J. Kang, L.-W. Wang, *J. Phys. Chem. Lett.* 2017, **8**, 489–493.
- 44 A. Waleed, M. M. Tavakoli, L. Gu, S. Hussain, D. Zhang, S. Poddar, Z. Wang, R. Zhang, Z. Fan, *Nano Lett.* 2017, **17**, 4951–4957.
- 45 H. Sun, W. Tian, F. Cao, J. Xiong, L. Li, *Adv. Mater.* 2018, **30**, 1–7.

View Article Online
DOI: 10.1039/C8NR09900F

Low-temperature Processed Inorganic Perovskites for Flexible Detectors with Broadband Photoresponse are successfully demonstrated. The modified one-step method based on solvent engineering technique was used to fabricate inorganic CsPbBr₃ perovskite films for flexible photodetectors (PDs). This device shows a broadband spectrum response from blind ultraviolet to visible light. Also the flexible perovskite detector exhibits excellent mechanical flexibility and improved environmental stability.

Keyword:

Flexible photodetectors, broadband spectrum response, Ohmic contact, mechanical flexibility

Low-temperature Processed Inorganic Perovskites for Flexible Detectors with Broadband Photoresponse

